



# On-chip implementation of the probabilistic quantum optical state comparison amplifier

DAVID W. CANNING,<sup>1</sup>  ROSS J. DONALDSON,<sup>1,\*</sup> SEBABRATA MUKHERJEE,<sup>1,3</sup>  ROBERT J. COLLINS,<sup>1</sup> LUCA MAZZARELLA,<sup>2</sup> UGO ZANFORLIN,<sup>1</sup> JOHN JEFFERS,<sup>2</sup> ROBERT R. THOMSON,<sup>1</sup> AND GERALD S. BULLER<sup>1</sup>

<sup>1</sup>Scottish Universities Physics Alliance, Institute of Photonics and Quantum Sciences, School of Engineering and Physical Sciences, Heriot-Watt University, David Brewster Building, Edinburgh EH14 4AS, UK

<sup>2</sup>Scottish Universities Physics Alliance, Department of Physics, University of Strathclyde, John Anderson Building, 107 Rottenrow, Glasgow G4 0NG, UK

<sup>3</sup>Current address: Department of Physics, The Pennsylvania State University, University Park, PA 16802, USA

\*[r.donaldson@hw.ac.uk](mailto:r.donaldson@hw.ac.uk)

**Abstract:** Propagation losses in transmission media limit the transmission distance of optical signals. In the case where the signal is made up of quantum optical states, conventional deterministic optical amplification schemes cannot be used to increase the transmission distance as the copying of an arbitrary and unknown quantum state is forbidden. One strategy that can offset propagation loss is the use of probabilistic, or non-deterministic, amplification schemes - an example of which is the state comparison amplifier. Here we report a state comparison amplifier implemented in a compact, fiber-coupled femtosecond laser-written waveguide chip as opposed to the large, bulk-optical components of previous designs. This pathfinder on-chip implementation of the quantum amplifier has resulted in several performance improvements: the polarization integrity of the written waveguides has resulted in improved visibility of the amplifier interferometers; the potential of substantially-reduced losses throughout the amplifier configuration; and a more compact and environmentally-stable amplifier which is scalable to more complex networks.

Published by The Optical Society under the terms of the [Creative Commons Attribution 4.0 License](https://creativecommons.org/licenses/by/4.0/). Further distribution of this work must maintain attribution to the author(s) and the published article's title, journal citation, and DOI.

## 1. Introduction

### 1.1. Background

The no-cloning theorem forbids the copying of an unknown quantum state [1] and gives rise to a minimum bound on the amount of noise that an ideal deterministic amplifier must necessarily add to a signal [2]. It also places a fundamental limit on the amount of information that an eavesdropper can extract from a signal composed of non-orthogonal states which is the foundation on which the security of quantum communications protocols is built [3]. For any communications protocol, classical or quantum, to be implemented in real-world applications, information carriers must be distributed over lossy communication channels and measured using imperfect detectors. Propagation loss and detector inefficiency both serve to reduce the maximum transmission range and decrease the communication rate. In the classical channels of fiber optic telecommunications networks, these loss mechanisms can be mitigated using deterministic amplification of the signal at periodic intervals throughout the channels. This solution is ineffective in the quantum domain - where the information carriers are single-photons or, more often, weak coherent states - as even

the minimum added noise of the ideal amplifier makes the amplified state useless for quantum communications purposes [4].

Probabilistic amplification aims to avoid the minimum noise requirement on an ideal deterministic linear amplifier by removing the requirement that the amplifier works every time [5]. The first probabilistic amplifier was devised by Ralph and Lund [6] based on Pegg et al.'s quantum scissors device [7]. It was implemented experimentally soon after their proposal [8,9] and probabilistic amplification has since developed into a burgeoning field of research. Ralph and Lund's amplifier is an example of a *phase-insensitive* probabilistic amplifier. Further work on quantum scissors style schemes followed [10–14] and other phase-insensitive probabilistic amplifiers have been proposed and implemented based on photon addition and subtraction [15–17], noise addition followed by photon subtraction [16–19], and weak measurement [20,21]. Phase-insensitive probabilistic amplifiers are fundamentally limited to operating at very low success probability in order to achieve high fidelity, however, *phase-sensitive* probabilistic amplifiers are subject to less stringent bounds [5]. Phase-sensitive probabilistic amplification schemes have been proposed based on unambiguous state discrimination [22] and state comparison amplification [23–25]. Most probabilistic amplification schemes generally try to herald successful amplification events via success criteria (measured by the amplifier), although non-heralded schemes have also been proposed such as the use of a non-heralded probabilistic amplifier to improve a signal nulling binary receiver [26].

In addition to the fundamental challenges, there are also practical challenges that quantum communications technologies must address; a commercially viable implementation of a quantum-enhanced device would ideally be scalable, modular, and standardized. Inspired by integrated electronics, there has been intense interest in recent years towards re-scaling quantum information protocols from bulk optical systems to the miniaturized area of integrated optical devices [27–29]. Integrated photonic components are inherently more compact and have the potential to be produced en masse in commercial fabrication facilities for relatively low cost.

There are a variety of different platforms that are being investigated for fabrication of integrated optical devices and each have their own benefits and drawbacks. The advanced infrastructure that has already been developed for the electronics industry makes it attractive to use silicon or III-V compound semiconductor systems. These techniques produce highly compact devices but they suffer from high propagation losses [28], and, while the technology for coupling electrical signals on- and off-chip is advanced, the same cannot be said for coupling of light which remains a non-trivial task due to the large size of a single-mode fiber core in comparison to the resultant waveguides [30]. These drawbacks are improved (at some cost) by using glass waveguides such as etched silica-on-silicon or writing waveguides directly into glass using femtosecond laser writing (FLW).

### 1.2. Femtosecond laser writing

FLW [31–33] is a laser-based manufacturing technique enabling fabrication of three-dimensional micro-optic structures inside transparent dielectric materials. Due to nonlinear absorption processes, focused sub-picosecond laser pulses can permanently change the refractive index of the material allowing the direct inscription of optical waveguides. The unique capabilities of this fabrication technique can facilitate the future development of many fields including telecommunication, astrophotonics, and nonlinear dynamics, as well as help us to understand various intriguing phenomena in photonic networks [34–36].

In the context of quantum optics, laser-inscribed components have been demonstrated to implement a variety of important quantum optical operations such as polarization-dependent [37] and polarization-independent [38] beamsplitters (generally referred to as *directional couplers* when on-chip), wave plates [39,40], and controlled phase shifts [41]. Auxiliary waveguides can also affect the local stress fields and ultimately give fine control to the primary waveguide's

birefringence and optical axis orientation [42]. In parallel with the technological developments described above, proof of principle quantum devices have been demonstrated using laser-written components, including quantum devices for state tomography [39], Hadamard [40] and CNOT [43] quantum logic gates, and integrated quantum memories in rare-earth-doped crystals [44].

FLW is a comparatively recent innovation and does not yet have the mature infrastructure of silicon and III-V manufacturing. However, it has the advantage that it can be used to create truly three-dimensional waveguide structures. Additionally, when using an appropriate beam-shaping method, FLW can produce waveguides with a circular cross-section [45], and therefore reduced birefringence, making the resulting waveguides highly suitable for applications that require the preservation of polarization and phase [28]. This fabrication technique provides excellent control over the shape of the fundamental mode, allowing for better mode matching and reduced on-chip coupling losses. Additionally, research has commenced into automation of the waveguide inscription process [46], offering the prospect of commercial manufacturing of multiple waveguide units in the future

No single platform currently provides the full range of capabilities required for all quantum information tasks and, for the moment, it is important to choose the platform that best suits the purposes of the device. We chose to implement the first on-chip implementation of the state comparison amplifier (SCAMP) using a FLW manufactured chip as the low birefringence of the waveguides ensured phase stability (crucial for state comparison of phase encoded states), the comparatively low coupling loss from fiber to the device maximized the effective intensity gain of the on-chip implementation, and the fast turnaround for creating prototypes aids investigation. This paper reports the first step towards fully on-chip state comparison amplification, which has been achieved by implementing the fundamental core beamsplitters of the amplifier in compact on-chip integrated directional couplers fabricated using FLW.

### 1.3. State comparison amplification

The SCAMP is a probabilistic amplifier operating on a known set of coherent state signals of arbitrary dimension. A case of interest for quantum communication is when the alphabet is composed of the states having the same mean photon number  $|\alpha|^2$  and whose phase belongs to the set  $\mathcal{A}_N = \{\phi_n\}$ , where  $1 \leq n \leq N$ ,  $n \in \mathbb{Z}^+$  and  $0 \leq \phi_n = \frac{2\pi}{N}(n-1) < 2\pi$  [23]. The amplifier consists of two stages: a *state comparison* stage, and a *photon subtraction* stage. In what we will refer to in what follows as the *standard SCAMP* setup [24], the state comparison stage consists of a single state-comparison operation and the photon subtraction stage consists of a single photon subtraction operation; this setup is summarized schematically in Fig. 1.

The *input* signal state which is to be amplified,  $|\alpha e^{i\phi_n}\rangle$ , has phase chosen uniformly at random from  $\mathcal{A}_N$ , with  $\alpha$  being real, and is incident at one input of a beamsplitter (with amplitude transmission and reflection coefficients given by  $t_1$  and  $r_1$  respectively and denoted  $B_{SC}$  in the figure). At the other input a *guess* coherent state is incident,  $|\beta_\phi\rangle$ , the amplitude of which is that of the input modified by a factor of  $t_1/r_1$ :

$$|\beta_\phi\rangle = |t_1 e^{i\phi} \alpha / r_1\rangle \quad \text{with} \quad \phi \in \mathcal{A}_N \quad (1)$$

where the phase  $\phi$  is chosen uniformly at random over the alphabet since there is no *a priori* knowledge on the probability distribution for the input signal. This beamsplitter combined with a single-photon detector (operating in Geiger mode) monitoring one of the output arms,  $D_0$ , forms the state comparison stage. In the case that the phase of the guess has been chosen correctly the state incident on the state comparison detector,  $D_0$ , is the vacuum state and the state output into the other mode is the input state amplified by a factor of  $1/r_1$ , i.e.  $|\alpha e^{i\phi_n}/r_1\rangle$ . On the other hand, coherent light will be routed to the detector if the amplifier guesses incorrectly causing it to possibly (but not necessarily) register an event. Thus, a success criterion can be defined as the condition that no detection event is registered at  $D_0$ .

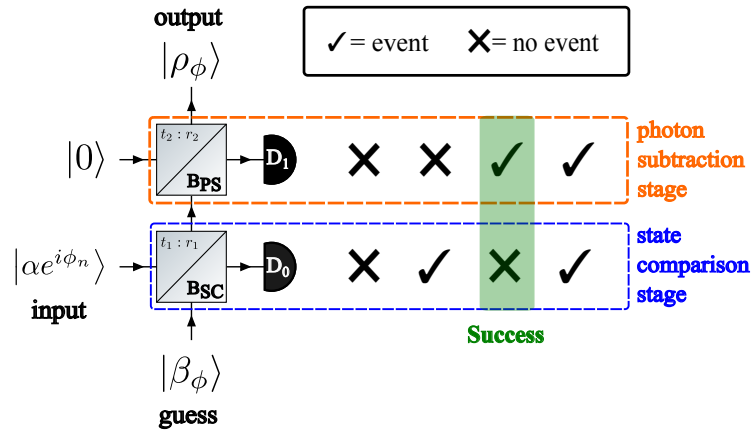


**Fig. 1.** Schematic representation of the standard SCAMP. When the phase of the input is guessed correctly the output of the SCAMP is the input state perfectly amplified by the nominal gain,  $g = \frac{t_2}{r_1}$ . The output is post-selected based on  $D_0$  registering no click and  $D_1$  registering a click to indicate the likelihood that the guess was correct.

In a practical system, non-unity detector efficiencies as well as the existence of the vacuum state in the coherent state superposition mean that the absence of a detection event does not allow us to infer with absolute certainty that light was not incident on the detector, i.e. that the guess was correct. This motivates the inclusion of the photon subtraction stage where the output of the state comparison stage is interfered with the vacuum at a second, highly transmitting, beamsplitter (with amplitude transmission and reflection coefficients given by  $t_2$  and  $r_2$  respectively, with  $t_2 \gg r_2$ , and denoted  $B_{PS}$  in the figure) [23]. One output mode is again monitored by a second single-photon detector  $D_1$ . The intensity of light incident on  $D_1$  is greatest for a correct guess meaning that a correct guess is more likely to cause a detection event at  $D_1$  than an incorrect guess. Thus, a second success criterion can be defined as the condition that a detection event is registered at  $D_1$ .

The other output of  $B_{PS}$  is taken to be the output of the SCAMP,

$$|\rho_\phi\rangle = |(r_1^2 + t_1^2 e^{i(\phi - \phi_n)})g\alpha e^{i\phi_n}\rangle \quad (2)$$

where the *nominal gain* of the standard SCAMP has been defined as  $g = t_2/r_1$ ; the *intensity gain* on the signal is given by the square of this value,  $g^2$ . We note that the output of the SCAMP is a perfect linear amplification of the input,  $|g\alpha e^{i\phi_n}\rangle$ , if (and only if) the guess was correct ( $\phi = \phi_n$ ) [2]. Without loss of generality we will set  $\phi_n = 0$  for the rest of the paper.

The running operation of the amplifier is then to condition the output signal based on having met both of the success criteria defined above. It is important to note that for all cases, except the special case where the state comparison beamsplitter is balanced ( $t_1 = r_1 = 1/\sqrt{2}$ ) and the phase alphabet is binary ( $N = 2$ ), there is still a non-zero probability of an incorrect guess that has met the first success criterion also meeting the second criterion. Furthermore, in a practical implementation an incorrect guess could meet both criteria even in the balanced binary case as the second success criterion could be met by a detector dark count or photons incorrectly routed due to experimental imperfections. Therefore, the output of the SCAMP, conditioned on the success criteria having been met, is still a statistical mixture of the perfectly amplified target state,  $|g\alpha\rangle$ , and the other possible output states corresponding to incorrect guesses and can be

described by the following density operator [23]

$$\hat{\rho}_S = \sum_{\phi \in \mathcal{A}_N} p_{\phi|S} |\rho_{\phi}\rangle \langle \rho_{\phi}| \quad (3)$$

where  $p_{\phi|S}$  is the probability that the conditioned output contains the state corresponding to the  $\phi$  guess. This probability can be related to the detection probability via Bayes' rule via the formula:

$$p_{\phi|S} = \frac{P_{S|\phi} P_{\phi}}{\sum_{\phi \in \mathcal{A}_N} P_{S|\phi} P_{\phi}}, \quad (4)$$

by estimating  $p_{S|\phi}$  by:

$$p_{S|\phi} = \left(1 - \frac{\tilde{C}_{\phi}^0}{R_{\phi}}\right) \frac{\tilde{C}_{\phi}^1}{R_{\phi}} \quad (5)$$

where the  $\tilde{C}_{\phi}^i$  are count rates corrected for the non-unity single-photon detection efficiency of the detectors and coupling losses, and the superscript  $i$  indicates the detector. The probability,  $p_{\phi}$ , that the amplifier guess is out of phase with the input by  $\phi$  is again uniformly over the alphabet since there is no *a priori* knowledge on the probability distribution for the input signal.

The standard SCAMP was first implemented experimentally with a nominal intensity gain  $g^2 = 1.8$  for evenly spaced phase alphabets of two-, four-, and eight-dimensions [24]. More recent work demonstrates a higher gain implementation with nominal intensity gain 11.9, investigates a non-standard SCAMP setup where the photon subtraction stage consists of more than one photon subtraction (increasing fidelity at cost of success rate), and shows SCAMP performance to be robust against environmental noise [25]. It is important to note that the true *effective intensity gain* of any implementation is suppressed by the component losses.

## 2. Experimental method

The setup for this experiment comprised two nested fiber-based Mach-Zehnder interferometers (MZIs) and was almost identical to that of previous bulk-optical implementations of the standard SCAMP [24,25]. For brevity, the full experimental description, along with a schematic diagram, is presented in Appendix A. Where this experiment differed from previous implementations of the SCAMP was in the implementation of the state comparison beamsplitter,  $B_{SC}$ , and the photon subtraction beamsplitter,  $B_{PS}$ . In previous implementations these were fiber-coupled standard bulk optical components whereas here we made use of a FLW manufactured waveguide chip.

For a systematic characterization, a complete three-waveguide-device (as illustrated schematically in Fig. 2) and an additional straight uncoupled waveguide were fabricated inside a 15-mm-long borosilicate glass (AF45) substrate. The glass substrate was mounted on air-bearing Aerotech x-y-z translation stages (ABL1000) and was translated at 6 mm/s through the focus (0.55 NA) of a 1-MHz train of circularly polarized sub-picosecond ( $\sim 350$  fs) laser pulses to fabricate each waveguide. The laser inscription parameters, such as translation speed, pulse energy and numerical aperture of the focusing lens, were optimized to produce low-loss waveguides that were single-mode and well confined for light at wavelengths near 850 nm wavelength.

The total insertion (propagation + bend + input/output coupling) loss was measured after aligning the device with commercially available V-groove arrays. The loss due to mode-mismatch was estimated to be less than 0.2 dB. The (average) on-chip loss for the waveguide(s) with one (two) directional coupler(s) was estimated to be 2.42 dB (4.58 dB). The on-chip propagation loss was estimated to be  $0.017 \text{ dBmm}^{-1}$  and the average losses associated with the directional couplers was estimated to be 2.28 dB per coupler.

The effective beam splitting ratios of the two directional couplers (after attachment of the V-grooves) were measured to be (12.5):(87.5) and (3.5):(96.5). As the waveguide structure of the

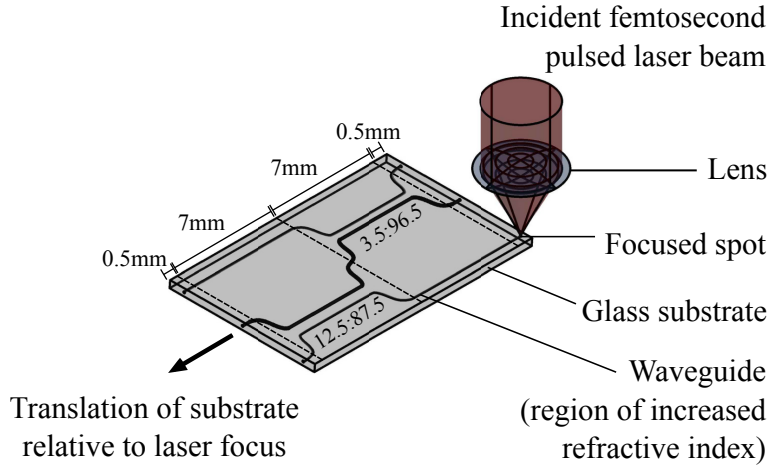


**Fig. 2.** Illustration of the FLW process for the waveguide chip used in this experiment. The two on-chip directional couplers are used as the implementation of the two beamsplitters,  $B_{SC}$  and  $B_{PS}$ , shown in Fig. 1. The symmetry of the waveguide structure allows for the chip to be integrated in two orientations.

chip is the same irrespective of which side of the chip is taken to be the input, we define two orientations of the chip. For clarity, this is the same as rotating the chip as shown in Fig. 5, so that the side of the chip that was previously the input now becomes the output, and vice versa. We define *orientation 1* in such a way that  $B_{SC}$  is the (12.5):(87.5) coupler and  $B_{PS}$  is the (3.5):(96.5) coupler. On reversing the input direction of the chip we define *orientation 2* such that  $B_{SC}$  is the (3.5):(96.5) coupler and  $B_{PS}$  is the (12.5):(87.5) coupler. Consulting the nominal gain of the standard SCAMP setup, orientation 1 (orientation 2) corresponds to a nominal intensity gain of 7.75 (25.09). The input-output coupling loss was estimated to be 1.70 dB on average.

The waveguide chip was integrated into the interferometric setup in both orientation 1 and orientation 2 where each orientation corresponds to an amplifier of different gain. Data was acquired for a binary ( $\mathcal{A}_2 = \{0, \pi\}$ ) and a four-dimensional ( $\mathcal{A}_4 = \{0, \pi/2, \pi, 3\pi/2\}$ ) phase alphabet. We present the visibility for both the binary and four-dimensional phase alphabet alongside the amplifier figures of merit for the four-dimensional alphabet in the bulk of the paper. The figures of merit for the binary alphabet are presented in Appendix B.

### 3. Analysis and results

Following the detailed model of [25], the experimentally measured count rates  $C_\phi$  are related to the idealised count rates,  $\tilde{C}_\phi$ , of Eq. (5) via:

$$\tilde{C}_\phi = R_\phi \left[ 1 - \left( \frac{R_\phi - C_\phi}{R_\phi} \right)^L \right] \quad (6)$$

where  $R_\phi$  is the laser pulse repetition rate multiplied by the *a priori* probability of an input  $\phi$  and  $L$  is the total intensity loss between the signal input and the detector (modelling imperfect detector efficiency as an additional source of loss). The corrected count rates can then be used to estimate the idealised intensity that is measured at each detector when the phase of the guess

differs from the input by  $\phi$

$$|D_\phi|^2 = \ln \left( \frac{R_\phi}{R_\phi - \tilde{C}_\phi} \right) \quad (7)$$

With these definitions, various figures of merit can be estimated for the SCAMP and plotted against the input mean photon number per pulse,  $|\alpha|^2$ , which for each measurement was then estimated from the count rates at the state comparison detector  $D_0$

$$|\alpha|^2 = \frac{1}{2Nt_1^2} \sum_{\phi \in \mathcal{A}_N} |D_\phi^0|^2 \quad (8)$$

In order to quantify the experimental imperfection in the inner MZI we modify the description of the guess state amplitude, Eq. (1), to add a phase mismatch term,  $\chi$

$$|\beta_\phi\rangle = \left| \frac{t_1}{r_1} \exp\{i(\phi + \chi)\} \alpha \right\rangle \quad (9)$$

We can estimate the cosine of the phase mismatch which corresponds to the visibility between a correctly guessed state and a guess state where the guess differs from the input by  $\pi$  [25]

$$\text{Visibility} = \cos(\chi) = \frac{|D_\pi^0|^2 - |D_0^0|^2}{|D_\pi^0|^2 + |D_0^0|^2} \quad (10)$$

The visibilities for both orientations of the chip are presented in Figs. 3(a) and 3(b) alongside values for a previously published [25] equivalent bulk optical implementation of standard SCAMP. We observe an increase in the achievable visibility for all values of  $|\alpha|^2$  for both the binary and four-dimensional phase alphabets. The increased visibility is especially pronounced in the four dimensional alphabet where we observe increased visibility on the order of 3.5%. This suggests improved polarization integrity in the waveguide chip when compared with the bulk optical components.

Further figures of merit for the SCAMP are presented in Figs. 4(a)–4(d) for the four-dimensional phase alphabet (relevant, for example, for phase implementations of the BB84 protocol [47] or quantum digital signatures [48,49]). The equivalent results for the binary alphabet are presented in Figs. 6(a)–6(d) in Appendix B. We first consider the overall *success rate* of meeting the success criteria, that is given by:

$$\text{Success Rate} = \sum_{\phi \in \mathcal{A}_N} R_\phi p_{S|\phi}, \quad (11)$$

where  $p_{S|\phi}$  has been defined in Eq. (4). The success rate is presented in Fig. 4(a), and increases with the mean photon number per pulse,  $|\alpha|^2$ , as expected.

Another two important figures of merit to assess the output quality are: the *correct state fraction* and *fidelity* with respect to the target state. The correct state fraction is the probability that the output contains the correct amplified state given that the detectors indicate success, i.e.  $p_{0|S}$  in our notation.

The fidelity with respect to the target state is given by  $F = \langle g\alpha | \hat{\rho} | g\alpha \rangle$  and can be seen as the probability of passing a measurement test on the device output, given success [23,25]. The latter quantities are not observables, but they can be estimated using the counts at the tomography detectors conditioned on success. In order to reconstruct the output state of the SCAMP (Eq. (3)) we estimate the number of pulses,  $N_\phi$ , that have met the success criteria for each value of the guess phase  $\phi$ . Following [23,25] the estimation of the  $N_\phi$  has been done via the counts at the

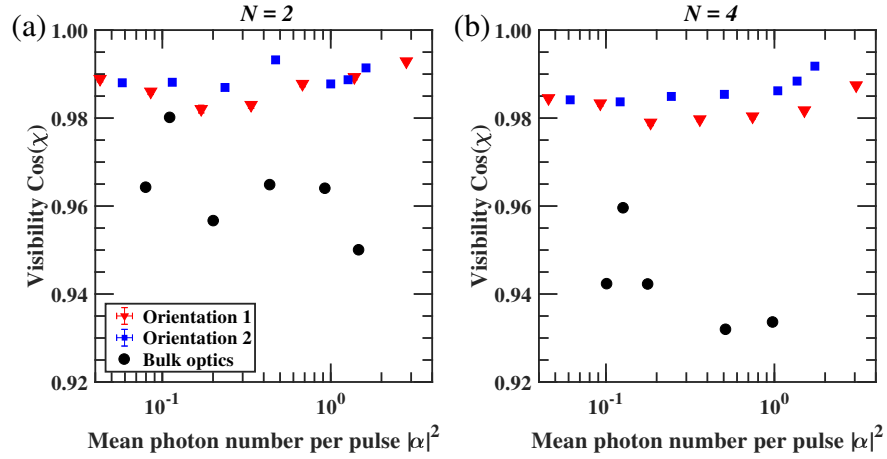


**Fig. 3.** Estimations of the cosine of the interferometric phase mismatch of the inner MZI. This quantity is interpreted as the visibility of the system and would equal one in a perfect system. The red triangles (blue squares) represent orientation 1 (orientation 2) of the waveguide chip. The black circles show the same quantity from a similar bulk optical experiment previously published in [25] for comparison. Each data point is the mean of 25 measurements and uncertainties were estimated by propagation of the standard error of the mean. Uncertainties are plotted for each data point but are in most cases smaller than the data point itself.

tomography detectors conditioned on success. The correct state fraction is thus given by:

$$p_{0|S} = \frac{N_0}{\sum_{\phi \in \mathcal{A}_N} N_\phi}, \quad (12)$$

while the fidelity is given by:

$$F = \sum_{\phi \in \mathcal{A}_N} \frac{N_\phi}{\sum_{\phi \in \mathcal{A}_N} N_\phi} |\langle g\alpha | \rho_\phi \rangle|^2, \quad (13)$$

We present the *correct state fraction*  $p_{0|S}$  in Fig. 4(b) as a function of  $|\alpha|^2$ . As is predicted by theory we observe that for all values of  $|\alpha|^2$  the correct state fraction exceeds the best achievable with *a priori* probability of  $1/N$  and increases towards unity with increasing input intensity. The fidelity is presented in Fig. 4(c) and displays an initial decrease with mean photon number per pulse followed by a recovery towards unity as predicted by the theory.

Finally, it is important to quantify the true gain that is achieved by the amplifier. The nominal intensity gain,  $g^2 = t_2^2/r_1^2$ , is suppressed by both the losses incurred by, and the imperfect visibility of, the amplifier. For this reason we quantify the *effective intensity gain* of the amplifier to be

$$g_{\text{eff}}^2 = g^2 L_{\text{SCAMP}} [t_1^4 + r_1^4 + 2t_1^2 r_1^2 \cos(\chi)] \quad (14)$$

where  $L_{\text{SCAMP}}$  is the loss of the SCAMP implementation between the input and the output of the device. Note that in case of unit visibility and of a lossless device, the expressions for the nominal intensity gain and the effective intensity gain coincide. This is presented in Fig. 4(d) for both the case where  $L_{\text{SCAMP}}$  is entirely on-chip (solid squares and triangles), and the case when  $L_{\text{SCAMP}}$  includes on-/off-chip coupling (empty squares and triangles). For orientation 1 (orientation 2) the mean effective intensity gain is 2.69 (8.73) when considering the amplification to be entirely

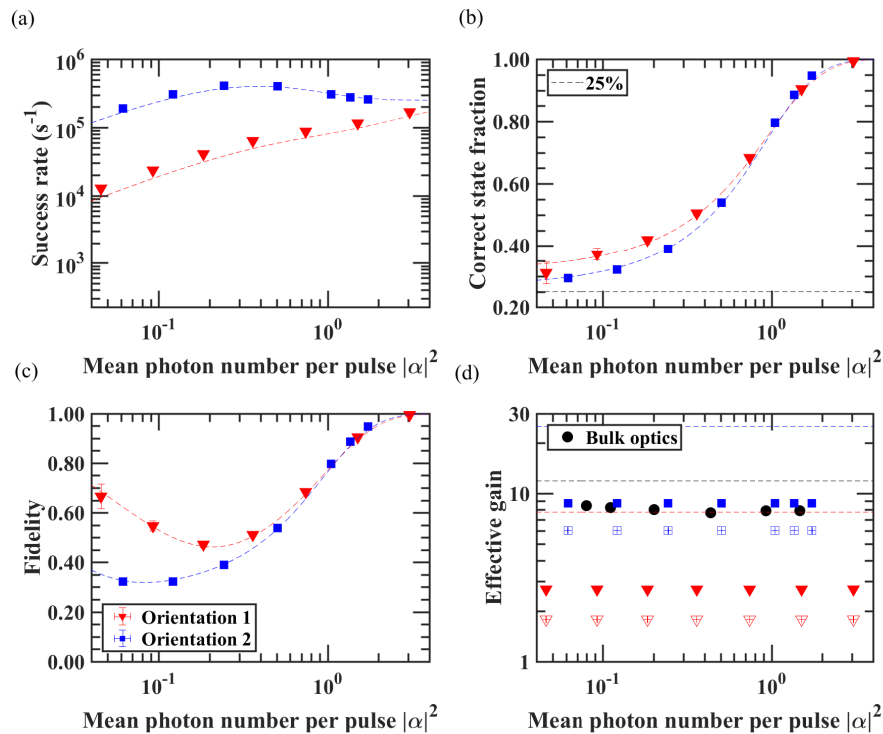


**Fig. 4.** Figures of merit for the SCAMP with four-dimensional ( $N = 4$ ) phase alphabet. (a) success rate; the rate at which both of the success criteria are met. (b) correct state fraction; weighting of the target state in the output ensemble. (c) fidelity; the overlap of the output mixture with the target state. (d) effective intensity gain; the nominal intensity gain ( $g^2 = t_2^2/r_1^2$ , shown by the dotted lines) suppressed by losses and imperfect visibility. The filled shapes represent the entirely on-chip gain omitting the loss incurred in taking the signal on- and off-chip. The empty shapes show the gain when accounting for on/off-chip loss. Equivalent values for a previously published bulk optical implementation are shown for comparison [25]. In all four plots the red triangles (blue squares) represent orientation 1 (orientation 2) of the waveguide chip. In (a), (b), and (c) the dashed lines show the theoretical predictions for the associated values using the theory of [23] assuming unity detection efficiency. Data points and uncertainties are calculated as described in Fig. 3

on-chip, and 1.72 (6.07) when on-/off-chip coupling is accounted for. For comparison, the equivalent bulk optical implementation ( $g^2 = 11.9$ ) has mean effective intensity gain of 8.20. The added suppression of the on-chip implementation is due to the increased on-/off-chip coupling when compared with a fiber splice, and the increased loss of the FLW manufactured directional couplers in comparison to the bulk optical components.

#### 4. Discussion

In this paper we have presented the results of two partially on-chip implementations of the SCAMP where a coherent state signal was coupled from fiber optics onto on-chip FLW manufactured waveguides, underwent on-chip coherent state amplification, before being coupled back into fiber. We observed increased visibility due to improved polarization integrity in the on-chip implementation when compared with an otherwise equivalent implementation that used commercially available fiber-coupled bulk optical components. This improved visibility is observed at the cost of decreased effective intensity gain due to increased losses introduced by this prototype version of the chip. The excess loss is, however, not prohibitive for the use of the amplifier on-chip as we have shown that, even accounting for coupling on and off chip, we can achieve similar gains to the bulk optical system, at a cost to fidelity, by varying transmission and reflection parameters. To be clear, we do not mean to say that fidelity is affected intrinsically by switching from bulk optics to the FLW chip. However, equivalent effective intensity gain can be achieved for the chip by compensating for any extra loss (when compared with bulk optics) by implementing a higher nominal intensity gain which, in turn, causes a decrease in fidelity as predicted by [23]. To quantify this for our particular chip, orientation 2 achieves an effective intensity gain of 6.07 from a nominal intensity gain of 25.09, whereas the similar effective intensity gain of 8.20 in [25] was achieved with a nominal intensity gain of 11.9. Strategies to recover the lost fidelity could include adding extra state comparisons (with feedforward state correction as demonstrated in [50]) or additional photon subtractions at a cost to the success rate. Our results clearly illustrate that any future technological improvements in coupling light on and off of integrated photonic platforms, as well as in minimizing bending loss introduced by the directional couplers would directly translate to an enhanced effective intensity gain in the SCAMP.

The amplifier could be further miniaturised by implementing any of the following on-chip alongside the waveguides: phase modulation of the guess signal [51], the stability tuning of the optical path length, dynamic tuning of the transmittance and reflectance of the directional couplers (coarse tuning could provide re-configurable gain), or on-chip integration of the single-photon detectors [52].

The SCAMP could perhaps be used as part of a more complex fully on-chip system to probabilistically recover signals that are already on chip (negating the added losses due to the coupling of light on and off chip). The SCAMP is highly customizable and the required effective intensity gain, fidelity, and success rate can be tailored (while respecting trade-offs) to a potential application. It can now also be said to be compatible with integrated photonic implementations and could potentially be leveraged in hybrid applications, for example fully optical quantum random number generation [53] or wavelength division multiplexed optical amplifier systems [54]. Furthermore, future work on non-coherent state comparison amplification will look to further explore the SCAMP's potential as a modular resource for quantum optical devices.

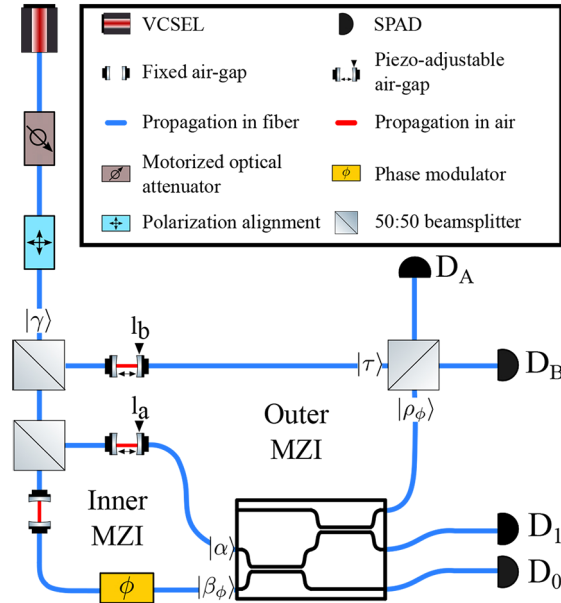


**Fig. 5.** A schematic representation of the experimental setup used in the partially on-chip SCAMP experiment. Note the symmetry of the chip on rotation by 180 degrees. By reversing the input and output ports of the chip it is possible to implement a SCAMP with a different nominal gain.

## Appendix A. Experimental setup

The experimental setup is shown schematically in Fig. 5. The initial source of coherent light,  $|\gamma\rangle$ , was a fiber-coupled vertical cavity surface-emitting laser (VCSEL) diode with a central wavelength of 848.2 nm, spectral linewidth (full width at half maximum) of 0.11 nm, and pulsed at a repetition rate of 1 MHz with pulse duration of 300 ps. This light was attenuated to a low mean photon number per pulse by a motorized optical attenuator before, using stress induced birefringence (via polarization controllers), the light emitted by the laser was aligned with the transmission axis of a 1000:1 extinction ratio fiber-coupled linear optical polarizer.

The light was then coupled into one input pigtail of a commercially available fiber-coupled bulk optical beamsplitter. This beamsplitter and all subsequent bulk optical components were fiber-coupled to fiber that was single-mode and polarization maintaining at the operational wavelength. The beamsplitter split the light into two identical lower amplitude weak coherent states at a balanced beamsplitter on entering the outer MZI. The state on the upper arm was retained as a reference state for the purpose of comparing the output state of the SCAMP with the idealized output state, or target state.

The state on the lower arm was again split by a second balanced beamsplitter on entering the inner MZI where the upper arm provided the input signal,  $|\alpha\rangle$ , which maintained a constant phase, and the lower arm was modulated by a phase  $\phi$  to form the guess signal. The phase modulation was performed with a lithium niobate phase modulator which varied the phase in a cyclical fashion from the discrete set of phases  $\mathcal{A}_N$ . Each of the four detectors,  $D_0$ ,  $D_1$ ,  $D_A$ , and  $D_B$ , was a commercial thick-junction silicon single-photon avalanche diode (SPAD) operating in Geiger mode with a mean detection efficiency of 41.5% whose electrical output was monitored by a picosecond resolution time-tagging module.

During initial setup a timing calibration procedure was performed on each interferometer to ensure high performance prior to loss balancing being performed between the arms of both interferometers. Next, in order to loss balance the inner MZI, each arm of the inner MZI was blocked in turn and the intensity at  $D_0$  was matched using the screw attenuator labelled  $l_a$ . This corresponds to ensuring that the guess amplitude,  $\beta_\phi$ , is related to the signal amplitude,  $\alpha$  by the expression given in Eq. (9). Then, in order to loss balance the outer MZI, each arm of the outer MZI was blocked in turn, while ensuring the intensity at  $D_0$  was minimized (corresponding to a correct guess,  $\phi = 0$ ) and the intensity at  $D_A$  and  $D_B$  was matched using the screw attenuator labelled  $l_b$ . This calibration procedure allows us to infer the relation of  $|\tau\rangle$ , to the target amplified state  $|\gamma\rangle$ .

The experiment was operated at various values of  $|\alpha|^2$  by varying the intensity of  $|\gamma\rangle$  using the motorized attenuator. Custom software dynamically tuned the optical length differences (via piezo-adjustable air-gaps) to maximize the observed visibility calculated between the  $\phi = 0$  and  $\phi = \pi$  pulses at  $D_0$  and the cross-visibility between the  $\phi = 0$  pulses at  $D_A$  and  $D_B$ . Minimum thresholds for these values were set at 97% and 90% respectively and a measurement would be discarded if they were not reached. Each data point plotted in this paper is an average of twenty-five individual single second integration measurements that achieved, or exceeded, these thresholds.

## Appendix B. Figures of merit for the binary phase alphabet

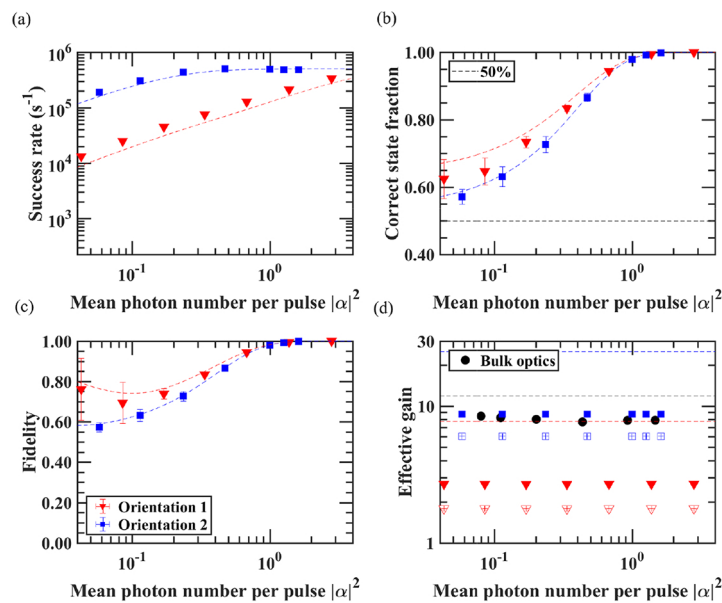


**Fig. 6.** Figures of merit for the SCAMP with binary ( $N = 2$ ) phase alphabet. Conventions are the same as in Figs. 4(a)–4(d). Data points and uncertainties are calculated as described in Fig. 3

## Funding

Engineering and Physical Sciences Research Council (EP/K015338/1, EP/M013472/1).

## Data availability

The data associated with this work can be downloaded from the Heriot-Watt data archive at <https://doi.org/10.17861/ce38b87b-001a-480f-b03c-f0be6e5dc3bd>

## Acknowledgments

S.M. and R.R.T. thank Debaditya Choudhury for assistance in experimental aspects.

## Disclosures

The authors declare no conflicts of interest.

## References

1. W. Wootters and W. Zurek, "A Single Quantum Cannot Be Cloned," *Nature* **299**(5886), 802–803 (1982).
2. C. M. Caves, "Quantum limits on noise in linear amplifiers," *Phys. Rev. D* **26**(8), 1817–1839 (1982).
3. V. Scarani, H. Bechmann-Pasquinucci, N. J. Cerf, M. Dušek, N. Lütkenhaus, and M. Peev, "The security of practical quantum key distribution," *Rev. Mod. Phys.* **81**(3), 1301–1350 (2009).
4. N. Gisin, G. Ribordy, W. Tittel, and H. Zbinden, "Quantum cryptography," *Rev. Mod. Phys.* **74**(1), 145–195 (2002).
5. S. Pandey, Z. Jiang, J. Combes, and C. M. Caves, "Quantum limits on probabilistic amplifiers," *Phys. Rev. A* **88**(3), 033852 (2013).
6. T. C. Ralph and A. P. Lund, "Nondeterministic Noiseless Linear Amplification of Quantum Systems," in *AIP Conf. Proc.*, vol. 1110 (2009), pp. 155–160.
7. D. T. Pegg, L. S. Phillips, and S. M. Barnett, "Optical State Truncation by Projection Synthesis," *Phys. Rev. Lett.* **81**(8), 1604–1606 (1998).
8. G. Y. Xiang, T. C. Ralph, A. P. Lund, N. Walk, and G. J. Pryde, "Heralded noiseless linear amplification and distillation of entanglement," *Nat. Photonics* **4**(5), 316–319 (2010).
9. F. Ferreyrol, M. Barbieri, R. Blandino, S. Fossier, R. Tualle-Broui, and P. Grangier, "Implementation of a Nondeterministic Optical Noiseless Amplifier," *Phys. Rev. Lett.* **104**(12), 123603 (2010).
10. J. Jeffers, "Nondeterministic amplifier for two-photon superpositions," *Phys. Rev. A* **82**(6), 063828 (2010).
11. N. Gisin, S. Pironio, and N. Sangouard, "Proposal for Implementing Device-Independent Quantum Key Distribution Based on a Heralded Qubit Amplifier," *Phys. Rev. Lett.* **105**(7), 070501 (2010).
12. C. I. Osorio, N. Bruno, N. Sangouard, H. Zbinden, N. Gisin, and R. T. Thew, "Heralded photon amplification for quantum communication," *Phys. Rev. A* **86**(2), 023815 (2012).
13. S. Kocsis, G. Y. Xiang, T. C. Ralph, and G. J. Pryde, "Heralded noiseless amplification of a photon polarization qubit," *Nat. Phys.* **9**(1), 23–28 (2013).
14. N. Bruno, V. Pini, A. Martin, and R. T. Thew, "A complete characterization of the heralded noiseless amplification of photons," *New J. Phys.* **15**(9), 093002 (2013).
15. J. Fiurášek, "Engineering quantum operations on traveling light beams by multiple photon addition and subtraction," *Phys. Rev. A* **80**(5), 053822 (2009).
16. P. Marek and R. Filip, "Coherent-state phase concentration by quantum probabilistic amplification," *Phys. Rev. A* **81**(2), 022302 (2010).
17. A. Zavatta, J. Fiurášek, and M. Bellini, "A high-fidelity noiseless amplifier for quantum light states," *Nat. Photonics* **5**(1), 52–56 (2011).
18. M. A. Usuga, C. R. Müller, C. Wittmann, P. Marek, R. Filip, C. Marquardt, G. Leuchs, and U. L. Andersen, "Noise-powered probabilistic concentration of phase information," *Nat. Phys.* **6**(10), 767–771 (2010).
19. J. Jeffers, "Optical amplifier-powered quantum optical amplification," *Phys. Rev. A* **83**(5), 053818 (2011).
20. D. Menzies and S. Croke, "Noiseless linear amplification via weak measurements," arXiv:0903.4181 [quant-ph] (2009).
21. J. Ho, A. Boston, M. Palsson, and G. Pryde, "Experimental noiseless linear amplification using weak measurements," *New J. Phys.* **18**(9), 093026 (2016).
22. V. Dunjko and E. Andersson, "Truly noiseless probabilistic amplification," *Phys. Rev. A* **86**(4), 042322 (2012).
23. E. Eleftheriadou, S. M. Barnett, and J. Jeffers, "Quantum Optical State Comparison Amplifier," *Phys. Rev. Lett.* **111**(21), 213601 (2013).
24. R. J. Donaldson, R. J. Collins, E. Eleftheriadou, S. M. Barnett, J. Jeffers, and G. S. Buller, "Experimental Implementation of a Quantum Optical State Comparison Amplifier," *Phys. Rev. Lett.* **114**(12), 120505 (2015).
25. R. J. Donaldson, L. Mazzarella, R. J. Collins, J. Jeffers, and G. S. Buller, "A high-gain and high-fidelity coherent state comparison amplifier," *Commun. Phys.* **1**(1), 54 (2018).
26. M. Rosati, A. Mari, and V. Giovannetti, "Coherent-state discrimination via nonheralded probabilistic amplification," *Phys. Rev. A* **93**(6), 062315 (2016).
27. S. Tanzilli, A. Martin, F. Kaiser, M. De Micheli, O. Alibart, and D. Ostrowsky, "On the genesis and evolution of Integrated Quantum Optics," *Laser Photonics Rev.* **6**(1), 115–143 (2012).

28. A. Orioux and E. Diamanti, "Recent advances on integrated quantum communications," *J. Opt.* **18**(8), 083002 (2016).
29. F. Flamini, N. Spagnolo, and F. Sciarrino, "Photonic quantum information processing: a review," *Rep. Prog. Phys.* **82**(1), 016001 (2019).
30. L. Vivien and L. Pavesi, *Handbook of Silicon Photonics* (Taylor & Francis, 2016).
31. K. M. Davis, K. Miura, N. Sugimoto, and K. Hirao, "Writing waveguides in glass with a femtosecond laser," *Opt. Lett.* **21**(21), 1729–1731 (1996).
32. R. R. Gattass and E. Mazur, "Femtosecond laser micromachining in transparent materials," *Nat. Photonics* **2**(4), 219–225 (2008).
33. D. Choudhury, J. R. Macdonald, and A. K. Kar, "Ultrafast laser inscription: perspectives on future integrated applications," *Laser Photonics Rev.* **8**(6), 827–846 (2014).
34. J. Bryant, R. R. Thomson, and M. J. Withford, "Focus issue introduction: recent advances in astrophotonics," *Opt. Express* **25**(17), 19966–19967 (2017).
35. M. Tillmann, B. Dakić, R. Heilmann, S. Nolte, A. Szameit, and P. Walther, "Experimental boson sampling," *Nat. Photonics* **7**(7), 540–544 (2013).
36. S. Mukherjee, D. Mogilevsev, G. Y. Slepyan, T. H. Doherty, R. R. Thomson, and N. Korolkova, "Dissipatively coupled waveguide networks for coherent diffusive photonics," *Nat. Commun.* **8**(1), 1909 (2017).
37. L. A. Fernandes, J. R. Grenier, P. R. Herman, J. S. Aitchison, and P. V. S. Marques, "Femtosecond laser fabrication of birefringent directional couplers as polarization beam splitters in fused silica," *Opt. Express* **19**(13), 11992–11999 (2011).
38. A. M. Streltsov and N. F. Borrelli, "Fabrication and analysis of a directional coupler written in glass by nanojoule femtosecond laser pulses," *Opt. Lett.* **26**(1), 42–43 (2001).
39. G. Corrielli, A. Crespi, R. Geremia, R. Ramponi, L. Sansoni, A. Santinelli, P. Mataloni, F. Sciarrino, and R. Osellame, "Rotated waveplates in integrated waveguide optics," *Nat. Commun.* **5**(1), 4249 (2014).
40. R. Heilmann, M. Gräfe, S. Nolte, and A. Szameit, "Arbitrary photonic wave plate operations on chip: Realizing Hadamard, Pauli-X, and rotation gates for polarisation qubits," *Sci. Rep.* **4**(1), 4118 (2015).
41. A. Crespi, R. Osellame, R. Ramponi, V. Giovannetti, R. Fazio, L. Sansoni, F. De Nicola, F. Sciarrino, and P. Mataloni, "Anderson localization of entangled photons in an integrated quantum walk," *Nat. Photonics* **7**(4), 322–328 (2013).
42. L. A. Fernandes, J. R. Grenier, P. R. Herman, J. S. Aitchison, and P. V. S. Marques, "Stress induced birefringence tuning in femtosecond laser fabricated waveguides in fused silica," *Opt. Express* **20**(22), 24103–24114 (2012).
43. A. Crespi, R. Ramponi, R. Osellame, L. Sansoni, I. Bongioanni, F. Sciarrino, G. Vallone, and P. Mataloni, "Integrated photonic quantum gates for polarization qubits," *Nat. Commun.* **2**(1), 566 (2011).
44. G. Corrielli, A. Seri, M. Mazzera, R. Osellame, and H. de Riedmatten, "Integrated Optical Memory Based on Laser-Written Waveguides," *Phys. Rev. Appl.* **5**(5), 054013 (2016).
45. M. Ams, G. Marshall, D. Spence, and M. Withford, "Slit beam shaping method for femtosecond laser direct-write fabrication of symmetric waveguides in bulk glasses," *Opt. Express* **13**(15), 5676–5681 (2005).
46. Y. Wang, L. Hermann Negri, I. Chiamenti, I. Abe, and H. J. Kalinowski, "Automated System for Femtosecond Laser Writing of Photonic Structures," *J. Control. Autom. Electr. Syst.* **29**(2), 153–162 (2018).
47. R. J. Hughes, G. L. Morgan, and C. G. Peterson, "Quantum key distribution over a 48 km optical fibre network," *J. Mod. Opt.* **47**(2-3), 533–547 (2000).
48. R. J. Collins, R. Amiri, M. Fujiwara, T. Honjo, K. Shimizu, K. Tamaki, M. Takeoka, E. Andersson, G. S. Buller, and M. Sasaki, "Experimental transmission of quantum digital signatures over 90 km of installed optical fiber using a differential phase shift quantum key distribution system," *Opt. Lett.* **41**(21), 4883–4886 (2016).
49. R. J. Collins, R. Amiri, M. Fujiwara, T. Honjo, K. Shimizu, K. Tamaki, M. Takeoka, M. Sasaki, E. Andersson, and G. S. Buller, "Experimental demonstration of quantum digital signatures over 43 dB channel loss using differential phase shift quantum key distribution," *Sci. Rep.* **7**(1), 3235 (2017).
50. R. J. Donaldson, L. Mazzarella, U. Zanforlin, R. J. Collins, J. Jeffers, and G. S. Buller, "Quantum state correction using a measurement-based feedforward mechanism," *Phys. Rev. A* **100**(2), 023840 (2019).
51. J. Thomas, M. Heinrich, P. Zeil, V. Hilbert, K. Rademaker, R. Riedel, S. Ringleb, C. Dubs, J.-P. Ruske, S. Nolte, and A. Tünnermann, "Laser direct writing: Enabling monolithic and hybrid integrated solutions on the lithium niobate platform," *Phys. Status Solidi A* **208**(2), 276–283 (2011).
52. F. Najafi, J. Mower, N. C. Harris, F. Bellei, A. Dane, C. Lee, X. Hu, P. Kharel, F. Marsili, S. Assefa, K. K. Berggren, and D. Englund, "On-chip detection of non-classical light by scalable integration of single-photon detectors," *Nat. Commun.* **6**(1), 5873 (2015).
53. U. Zanforlin, R. J. Donaldson, R. J. Collins, and G. S. Buller, "Analysis of the effects of imperfections in an optical heterodyne quantum random-number generator," *Phys. Rev. A* **99**(5), 052305 (2019).
54. D. Malik, G. Kaushik, and A. Wason, "Performance evaluation of hybrid optical amplifiers in WDM system," *J. Opt.* **47**(3), 396–404 (2018).